Friction and Wear of Metals under Micro-abrasion, Wet and Dry Sliding Conditions

Cesar David Resendiz-Calderon, Leonardo Israel Farfan-Cabrera ⓘ, Joaquín Esteban Oseguera-Peña, Irving Cázares-Ramírez, and Ezequiel Alberto Gallardo-Hernandez

This work aims to characterize and compare the coefficient of friction (CoF) and wear rates of some metallic materials (AISI 6061-T6 alloy, AISI 316 L stainless steel and ASTM F1537 CoCrMo alloy) under different wear modes, namely, micro-abrasion abrasion (rolling and mixed rolling/grooving abrasion), and wet and dry sliding abrasion. The wear modes were achieved by conducting testing under muddy environment at different SiC abrasive particles concentration and wet and dry conditions at three different loads (1, 2 and 3 N) using an instrumented micro-abrasion tester. Wear volumes were measured by optical profilometry to estimate wear rates, while wear patterns were visualized in detail by SEM. CoF, wear rate and mode results for all materials and conditions are reported and discussed. Wear modes were found to have a considerable effect on CoF and wear rate for the materials. Pure rolling abrasion generated the highest wear rates for all materials. Mixed rolling abrasion/grooving produced higher CoFs, but lower wear rates than those produced by pure rolling abrasion. Wet sliding promoted the highest CoFs for AISI 316L SS and AISI 6061-T6 meanwhile dry sliding generated the lowest CoFs and wear rates.

1. Introduction

The micro-abrasion wear test is a suitable method used for characterization and evaluation of wear rate and resistance of a wide range of materials, namely, metals (Ref 1-3), ceramics (Ref 4-7), polymers (Ref 8, 9) and thin coatings (Ref 10-12) under rolling abrasion mechanism. The method basis is to produce a wear crater with defined geometry, commonly spherical or ellipsoid cap, on a small and thin flat specimen by loading it against a rotary hard ball, usually with 25.4 mm in diameter, in presence of an abrasive slurry made of deionized water and hard abrasive particles (4-8 μm) (Ref 13, 14). The advantage of this test is the formation of defined small wear scars (micro-scale) with rolling abrasion patterns and, in some cases, plowing or grooving features depending on some testing conditions (Ref 15-17). Both are variants from micro-abrasive wear depending on the dynamics of the abrasive particles which can involve rolling of the particles at the interface (rolling abrasion) or sliding of the abrasive particles at the interface (grooving or plowing) (Ref 15, 18-20). Rolling abrasion is produced by free hard micro-particles rolling at the sliding interface promoting commonly numerous micro-indentations with ductile or brittle behavior in the scar as wear feature (Ref 20), while plowing or grooving is generated by the asperities or/and hard micro-particles fixed at one counterface sliding against the other. The main wear feature of plowing or grooving is the formation of micro-grooves or scratches inducing the mechanisms of micro-cutting, micro-plowing and micro-cracking along the scar in the sliding direction. Besides, some materials, commonly soft materials at high loads and large abrasive particles, are prone to exhibit ridging in micro-abrasion tests (Ref 9, 14, 15, 17, 21). Ridging or ridge formation is caused because the abrasive particles fail to become fully entrained into the wear contact but instead flow around the sides promoting an unworn region in the scar aligned parallel to the sliding direction (Ref 22). Those wear patterns are difficult to obtain with acceptable reproducibility in other testers. Since the micro-abrasion wear test was introduced by Rutherford and Hutchings in 1996 (Ref 13), a great amount of work has been done to improve the test reproducibility and to implement it as a standard wear test method (Ref 22-29). Taking advantage of the accuracy and effectiveness of this test, different research groups (Ref 30-40) have modified the tester and procedure implementing additional devices to carry out friction measurements and corrosion analysis as complement for deeper explorations.

The measurement of friction to estimate the corresponding coefficient of friction (CoF) of materials in a micro-abrasion test is a significant contribution. This idea was firstly proposed and reported by Gee and Wicks in 2000 (Ref 30). They measured tangential forces (friction force) of some coatings including TiN, DLC and CrN under dry sliding condition in a micro-abrasion tester with fixed ball configuration. They found the tester modification to be very effective to evaluate CoF behavior of those coatings. In 2009, Cozza et al. (Ref 31) studied the influence of constant pressures on the CoF of an AISI H10 steel in a micro-abrasion tester. They used a solution of deionized water with suspended 3μm SiC particles as abrasive slurry for the tests. They found that constant applied

Cesar David Resendiz-Calderon, Leonardo Israel Farfan-Cabrera, Joaquín Esteban Oseguera-Peña, and Irving Cázares-Ramírez, Tecnologico de Monterrey, Escuela de Ingeniería y Ciencias, Ave. Eugenio Garza Sada 2501, Monterrey, NL 64849, Mexico; and Ezequiel Alberto Gallardo-Hernandez, Instituto Politécnico Nacional, SEPI-ESIME Zacatenco, Mexico City, DF 07738, Mexico. Contact e-mail: farfanl@hotmail.com.

pressures reduce variation in friction. Also, CoF was found to decrease as the degree of micro-rolling abrasion increases. Afterward, using the same test equipment, Cozza et al. (Ref 32) investigated the effects of hardness on CoF and wear rates for TiN and TiC coatings deposited in an AISI D2 steel. They found that hardness did not have influence on the CoF. Later, in a similar research, Cozza et al. (Ref 33) examined the influence of applied load and concentration of abrasive particles on CoF behavior of an AISI H10 steel. They concluded that neither applied loads and abrasive concentration have influence on CoF for the material and test conditions used in their investigation. More recently, Peng et al. (Ref 34) used a modified micro-abrasion tester to evaluate wear resistance and CoF behavior of a Mn16 steel in simulated iron ore mill conditions. The tests were conducted under dry sliding conditions, in presence of iron ore powder, and using a slurry made of iron ore powder with distilled water. They reported that CoF increases when applied load increases if no abrasive particles are present, while CoF decreases if abrasive particles are present. They also found that applied load has major influence in CoF than the rotational speed of the counterpart.

Despite the above attempts to measure and report CoF of different materials under different contact conditions in a micro-abrasion tester, the method has not explored broadly for this purpose. Also, CoF and wear rates for most materials have not been investigated under different micro-abrasion wear modes, namely, rolling abrasion and mixed rolling abrasion/grooving. Thus, the aim of this work is to contribute with a broader study to characterize and compare CoF and wear rate of some metallic materials (AISI 6061-T6, AISI 316 L SS and ASTM F1537 CoCrMo) under different wear modes, namely, both variants of micro-abrasion (rolling abrasion, mixed rolling abrasion/grooving), and wet and dry sliding abrasion.

2. Experimental Procedure

2.1 Materials and Sample Preparation

4 mm thickness samples were cut from 25.4 mm diameter bars of three different materials (AISI 6061-T6, AISI 316 L SS and ASTM F1537 CoCrMo) and polished to have a roughness of R_a = 0.03 ± 0.01 μm. AISI 52100 steel balls (diameter 25.4 mm) were used as counterface for all tests. They were etched in a mixture of nitric acid (30 vol.%) and ethyl alcohol (70 vol.%) to generate a pitting surface with a mean surface roughness, S_a and R_a of 0.4 ± 0.05 μm for all the balls. The surface roughness, in terms of S_a and R_a, was measured by an optical profilometer. The surface conditioning is suggested in the original micro-abrasion method to obtain acceptable reproducibility of rolling micro-abrasive mechanisms and consistent wear rates (Ref 22). Recently, Costa et al. (Ref 41) have found that different ball's surface topography/roughness, in terms of S_a, can promote differences in the dynamics of the abrasive particles and therefore on micro-abrasion coefficients. So, it is important to control as much as possible the surface roughness of balls for micro-abrasion tests. The materials to be tested were chosen to evaluate materials with different mechanical properties (AISI 6061-T6 – high ductility/low hardness, AISI 316 L SS - Medium ductility/medium hardness, and ASTM F1537 CoCrMo - low ductility/high Hardness) and possessing high corrosion resistance to curtail effects of corrosion on wear and

friction results. The hardness and Young's modulus values of the materials are in Table 1. They were obtained by Vickers depth-sensing indentation tests by using an applied load of 300 mN and then calculated by following the Oliver-pharr method (Ref 42).
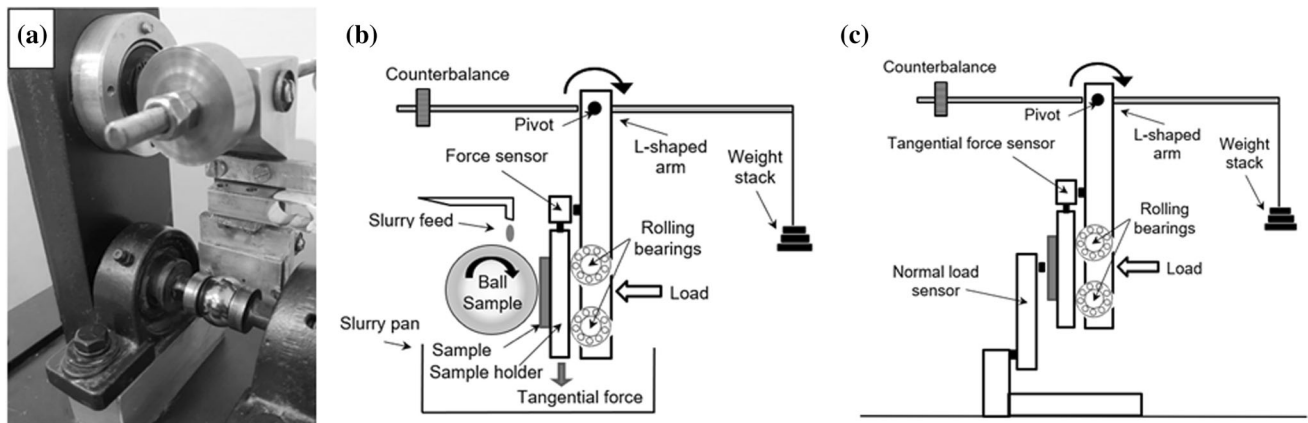
2.2 Test Set-Up and Conditions

The tests were carried out using a homemade apparatus with a fixed ball micro-abrasion tester configuration. A photograph and schematic diagrams of the test set-up arrangement are shown in Fig. 1a-c. Basically, the test is to load a flat material specimen against a rotating steel ball with predefined normal force, speed and cycles to produce sliding contact under specific conditions. Either an abrasive slurry or water are dripped continuously onto the ball and entrained into the contact interface by the ball rotary effect for the micro-abrasion or wet conditions, respectively. In the tester, the steel ball sample is clamped between two coaxial driving shafts rotated by an electric motor. The electric motor is controlled to rotate at constant speed and specific ball cycles or testing time through an encoder with 0.75° of rotation precision connected to a USB-6009 data acquisition (DAQ) device. The material specimen is held in a plate (sample holder) located at the bottom of the pivoted L-shaped arm. The plate is fixed to one end of a 1 kg load sensor (straight bar weight sensor), while the other end of the sensor is fixed to a metallic support which is also fixed to the L-shaped arm. Besides, the back of the plate is contacted to rolling bearings fixed in the L-shaped arm. This allows the plate to move freely in the vertical direction limiting horizontal displacements. The load sensor is also connected to the USB-6009 data acquisition (DAQ) device and a computer for monitoring and acquiring the tangential force generated by friction produced by the steel ball sample that slides against the flat material sample. CoF was calculated by Eq 1 where F_f is the friction force measured with the load cell, while N is the normal applied load.

$$\mu = \frac{F_f}{N} \qquad \text{(Eq 1)}$$

The L-shaped arm is balanced by the counterbalance before the load is applied via dead-weight from a horizontal lever. An extra load sensor with similar specifications to those from the tangential force sensor is installed to measure and acquire the normal load applied to the material sample before the test, and then it is removed to locate the steel ball and start the test. It is very useful to assure statically the load applied to the contact. The test conditions are in Table 2. Muddy conditions were conducted by using two slurries with different abrasive particles concentrations to achieve pure rolling abrasion and rolling abrasion combined with grooving, respectively. One slurry was made of deionized water with F-1200 SiC particles with hardness of $H_V = 25.5$ GPa and size of 4 − 8 μm at a

Table 1 Mechanical properties of the used materials

Sample material	Hardness, GPa	Young's modulus, GPa
AISI 6061-T6	1	69
AISI 316 L SS	4.8	200
ASTM F1537 CoCrMo	7.8	241
AISI 52100 steel balls	3.7	210

Fig. 1 (a) Photograph of the tester; (b) Schematic view of the instrumented micro-abrasion test set-up; (c) Schematic view of the instrumented load sensor in the test set-up

Table 2   Test conditions

Parameter	Muddy at a high abrasive particles concentration (MHC)	Muddy at a low abrasive particles concentration (MLC)	Wet	Dry
Wear mode	Rolling abrasion	Mixed rolling abrasion/grooving	Wet sliding abrasion	Dry sliding abrasion
Load (N)	1, 2, 3	1, 2, 3	1, 2, 3	1, 2, 3
Sliding distance (m)	20	20	20	20
Abrasive media or fluid	Abrasive slurry 80gr /100 ml	Abrasive slurry 20 gr/100 ml	Deionized water	...
Sliding speed (m/s)	0.1	0.1	0.1	0.1

concentration of 80 gr/100 ml for the high abrasive concentration (MHC) tests meanwhile the other slurry was prepared at an abrasive particles concentration of 20 gr/100 ml for the low abrasive concentration (MLC) tests. The micro-SiC particles are recommended and widely used for caring out characterization of materials through conventional micro-abrasion tests (Ref 28). Apart of using common abrasive particles for micro-abrasion testing, it was selected to obtain a first overview of CoF variation by the wear mechanism (rolling and grooving), but not by varying the abrasive particles material. These particles were pure deionized water was applied to the contact for wet tests meanwhile no slurry or deionized water were used for the dry tests. Preliminary tests were carried out to determine the wear steady-state for each test condition. It was found that wear rate for all the conditions reached stability after 15 m of sliding distance. So, 20 m sliding distance was chosen for all tests. The tests were run at three different normal loads (1, 2 and 3 N) and constant speed of 0.1 m/s. A new ball (conditioned) was used for each test. The sliding distance was selected since friction and wear steady-state was reached and minimal ball surface roughness, $S_a \leq 0.05$ μm, variation was produced for all the conditions tested. Three repetition tests were carried out for each condition. So, the corresponding standard deviation from the three friction and wear measurements was obtained and reported for each condition. The wear scars generated were visualized in detail by scanning electron microscopy (SEM) and measured in an optical profilometer to determine wear volumes.

3. Results and Discussion

3.1 Coefficient of Friction and Wear Under Rolling Abrasion

Figure 2a-d shows the average values of CoF and wear rates obtained at 1, 2 and 3 N, and the CoF behaviors for 1 and 3 N for the materials tested under MHC conditions. Figure 3 a-c shows SEM images from the typical wear scars obtained for each material by testing at 3 N since they can be considered as the most representative. Wear rates measured in mm^3/m units were compared for the materials and the different loads tested instead of reporting the specific wear rate values (mm^3/Nm). The first is useful when wear behavior with load is unknown or different wear mechanisms transition are expected meanwhile the last one is more commonly used for distinguishing the wear resistance property of different materials assuming or meeting wear rates proportional to load according to Archard wear equation described in (Ref 43). The AISI 6061-T6 alloy presented the highest CoF values from 0.44 for applied loads of 1 and 2 N to 0.56 for 3 N meanwhile the AISI 316L SS and ASTM F1537 CoCrMo alloy presented lower average values of 0.37 and 0.39, respectively. CoF of AISI 6061-T6 was risen significantly (from 0.44 to 0.56) with load increase, while CoF of AISI 316L SS and ASTM F1537 CoCrMo had a minimal growth with load increase. The wear scars of all the materials exhibited pure rolling abrasion features, namely, micro-indentations. However, the scars generated in the AISI 6061-T6 presented substantial amounts of embedded SiC particles at 3 N as identified by EDS analyses as shown in
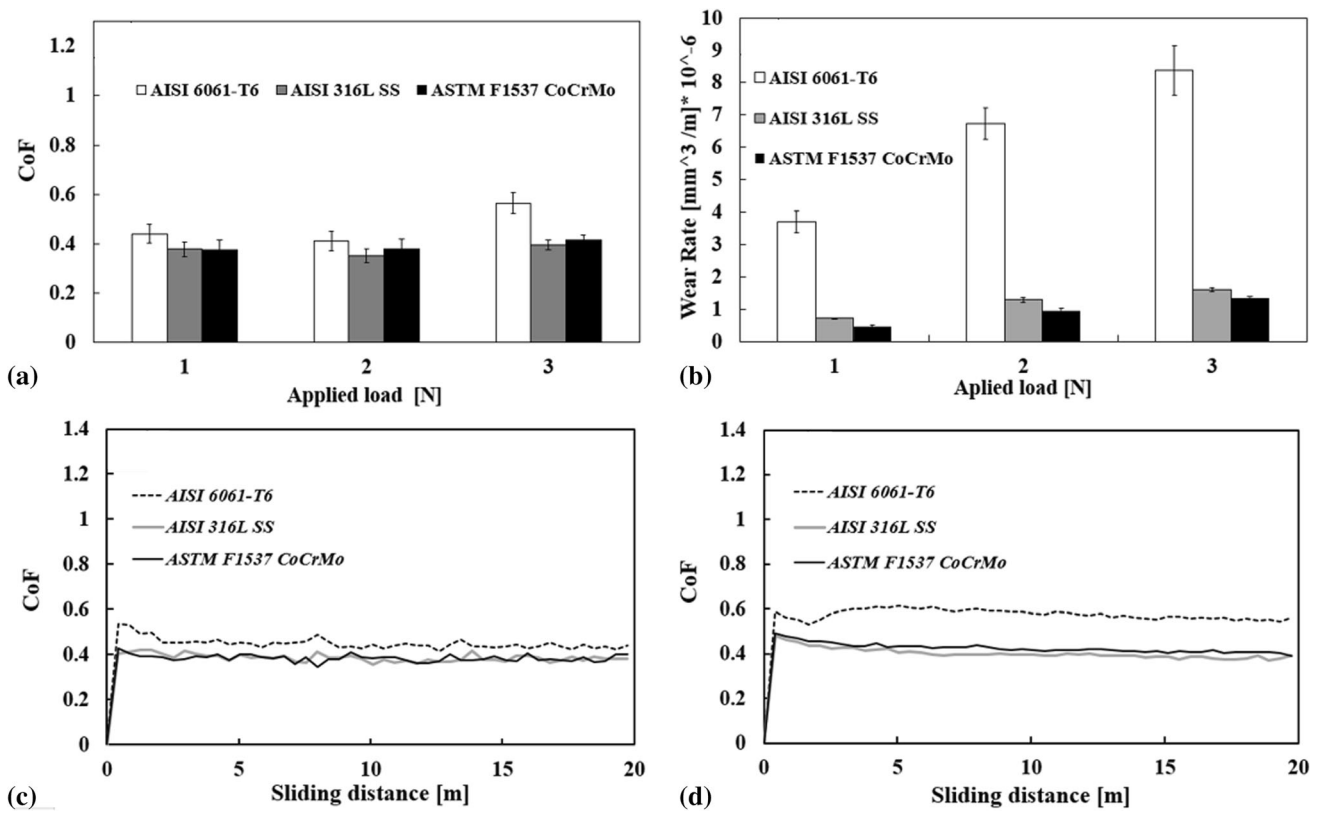
Fig. 2 (a) Average CoF for the different loads under MHC condition; (b) Wear rates for the different loads under MHC condition; CoF behavior for MHC condition (c) 1 N; (d) 3 N
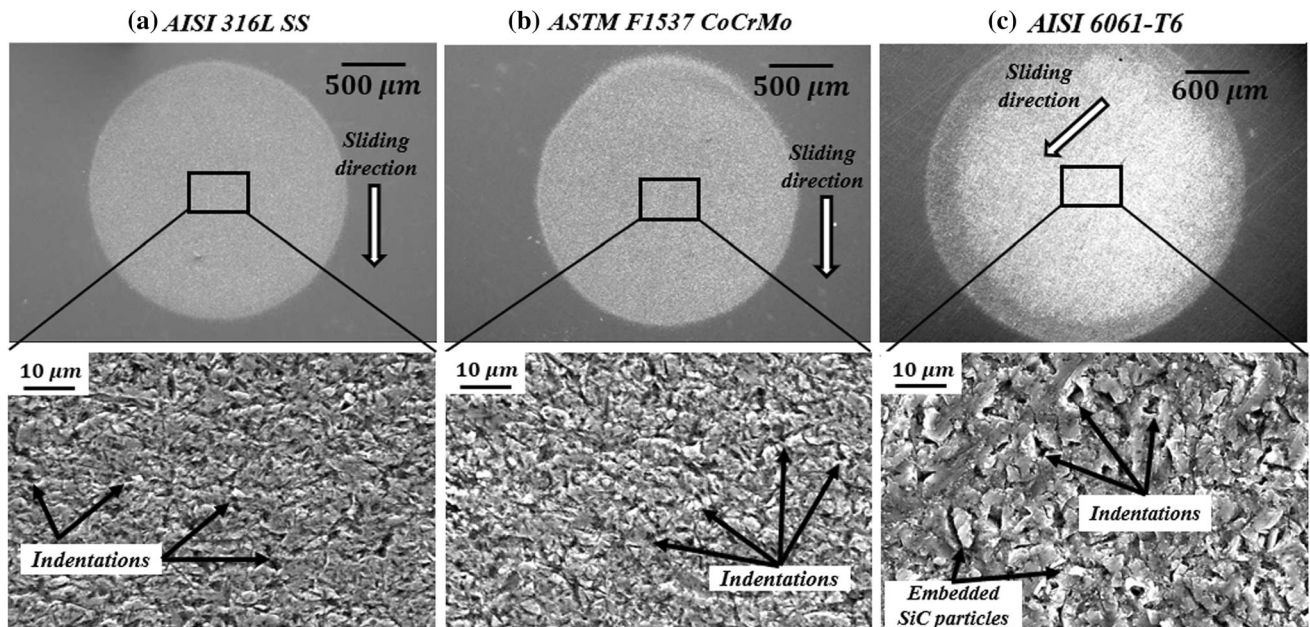
Fig. 3 SEM images from typical wear scars obtained under MHC condition for the materials at 3 N: (a) AISI 316L SS; (b) ASTM F1537 CoCrMo; (c) AISI 6061-T6

Fig. 4. It is due to its low hardness promoting easier and deeper SiC indentations and embedment. The CoF increase obtained for AISI 6061-T6 at 3 N was related to the large amount of SiC particles embedment. Those embedded particles in the scar do not roll, but they abrade the steel ball surface in some extent as

an effect of two-body-abrasion mechanism generating higher shear forces. All materials exhibited a wear rate increase with load which was proportional in some cases. The ASTM F1537 CoCrMo and AISI 6061-T6 presented the lowest and highest wear rates, respectively. The ASTM F1537 CoCrMo presented
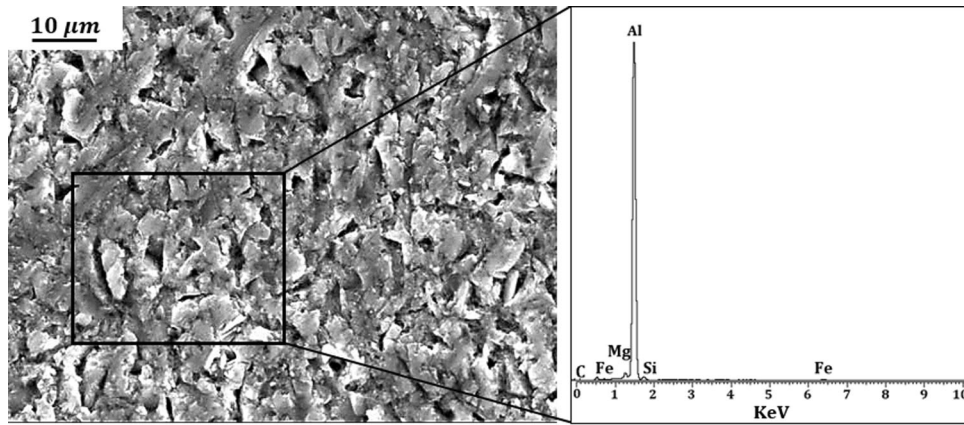
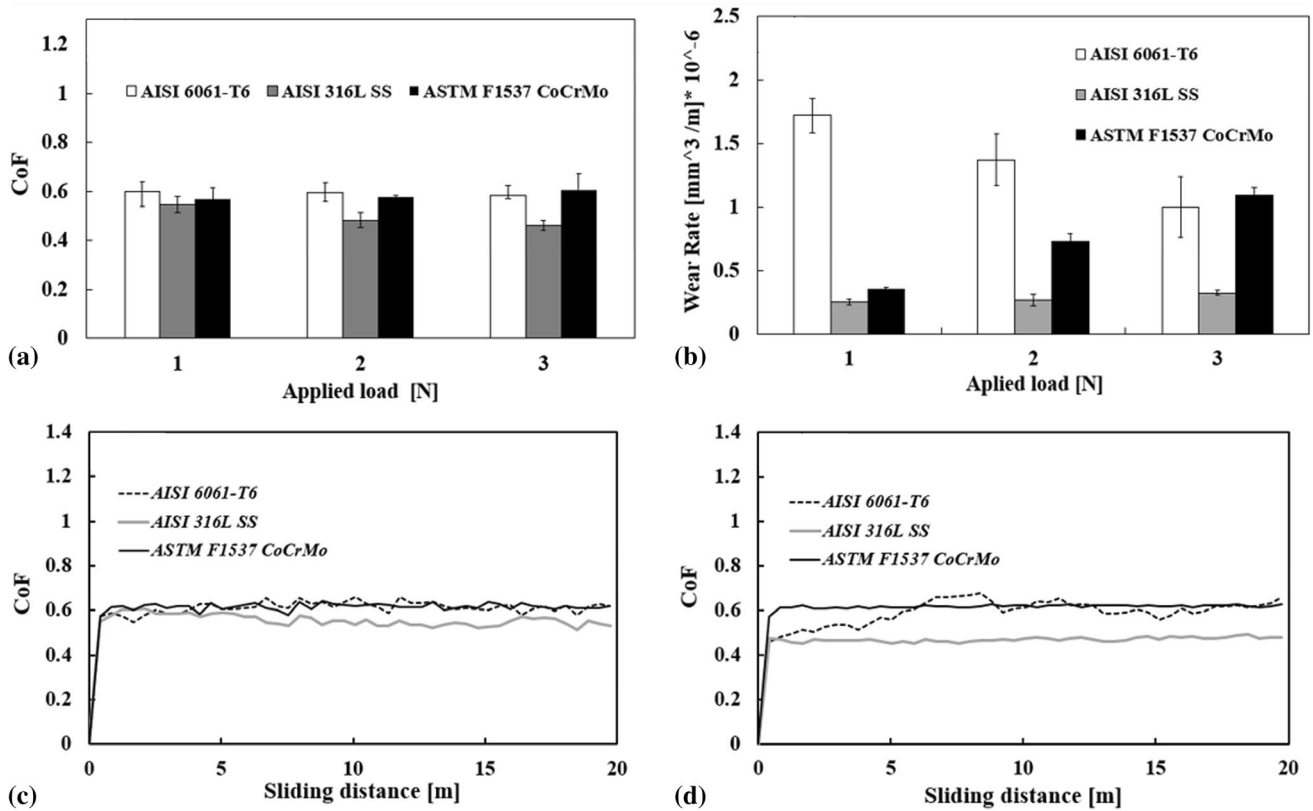**Fig. 4** EDS analysis over AISI 6061-T6 Aluminum alloy for MHC condition

Fig. 5 (a) Average CoF for the different loads under MLC condition; (b) Wear rates for the different loads under MLC condition; CoF behavior for MLC condition (c) 1 N; (d) 3 N

values ranging from 4.6×10^{-7} mm^3/m at 1 N to 13.4×10^{-7} mm^3/m at 3 N, while AISI 6061-T6 exhibited values from 37×10^{-7} mm^3/m at 1 N to 83.7×10^{-7} mm^3/m at 3 N. It is ascribed to the high hardness of ASTM F1537 CoCrMo and the low hardness of AISI 6061-T6, respectively.

3.2 Coefficient of Friction and Wear Under Mixed Rolling Abrasion/Grooving

The average CoF and wear rate values at 1, 2 and 3 N, and the CoF behaviors for 1 and 3 N obtained for the materials tested under MLC condition are shown in Fig. 5a-d. The SEM images from the typical wear scars obtained for the materials

tested at 3 N are illustrated in Fig. 6a-c. The wear patterns generated at MLC were different than MHC only for ASTM F1537 CoCrMo and AISI 316L SS for the three loads tested as expected. Grooving marks with few indentations caused by rolling abrasion were the characteristic patterns found. This mixed process occurs when a significant proportion of the particles are embedded in the surface of the ball or dragged by the ball asperities acting as fixed indenters, as also reported in (Ref 22, 44). So, it generates a series of fine parallel grooves in the specimen surface. Besides, free particles roll at the interface also promoting micro-indentations (rolling abrasion). In contrast, aluminum alloy´s scars exhibited mainly micro-indentations with large amounts of embedded SiC particles like those
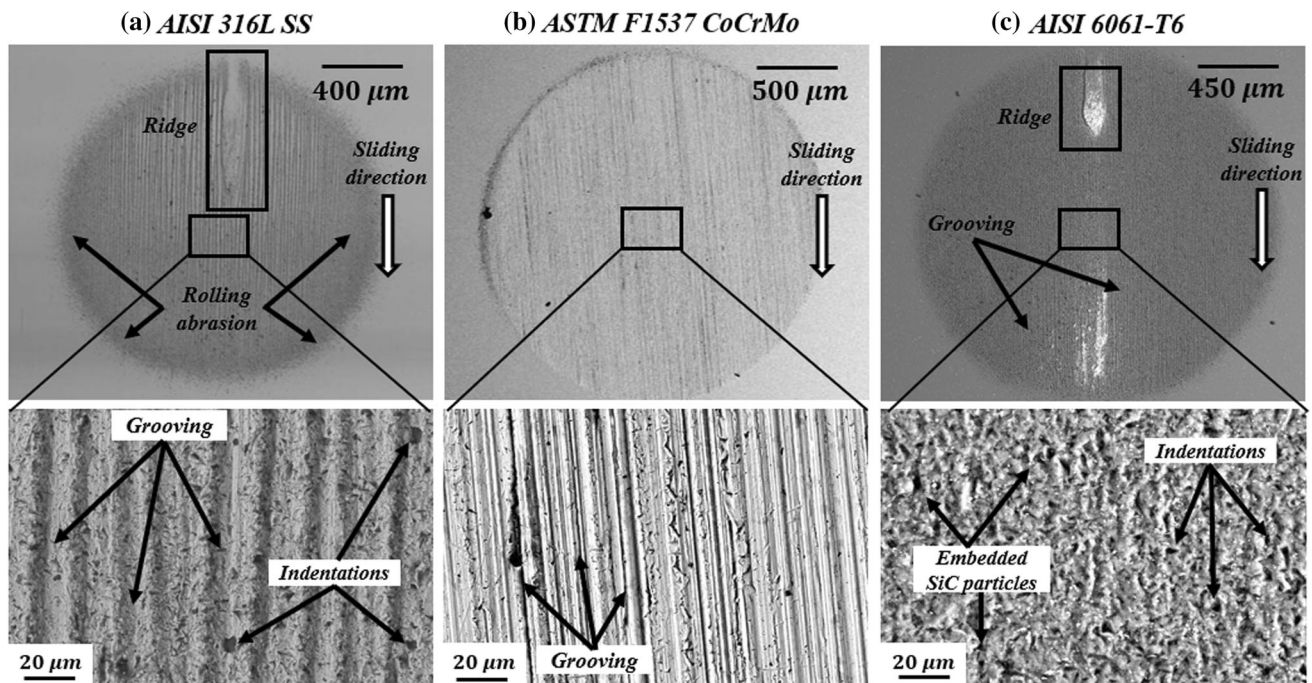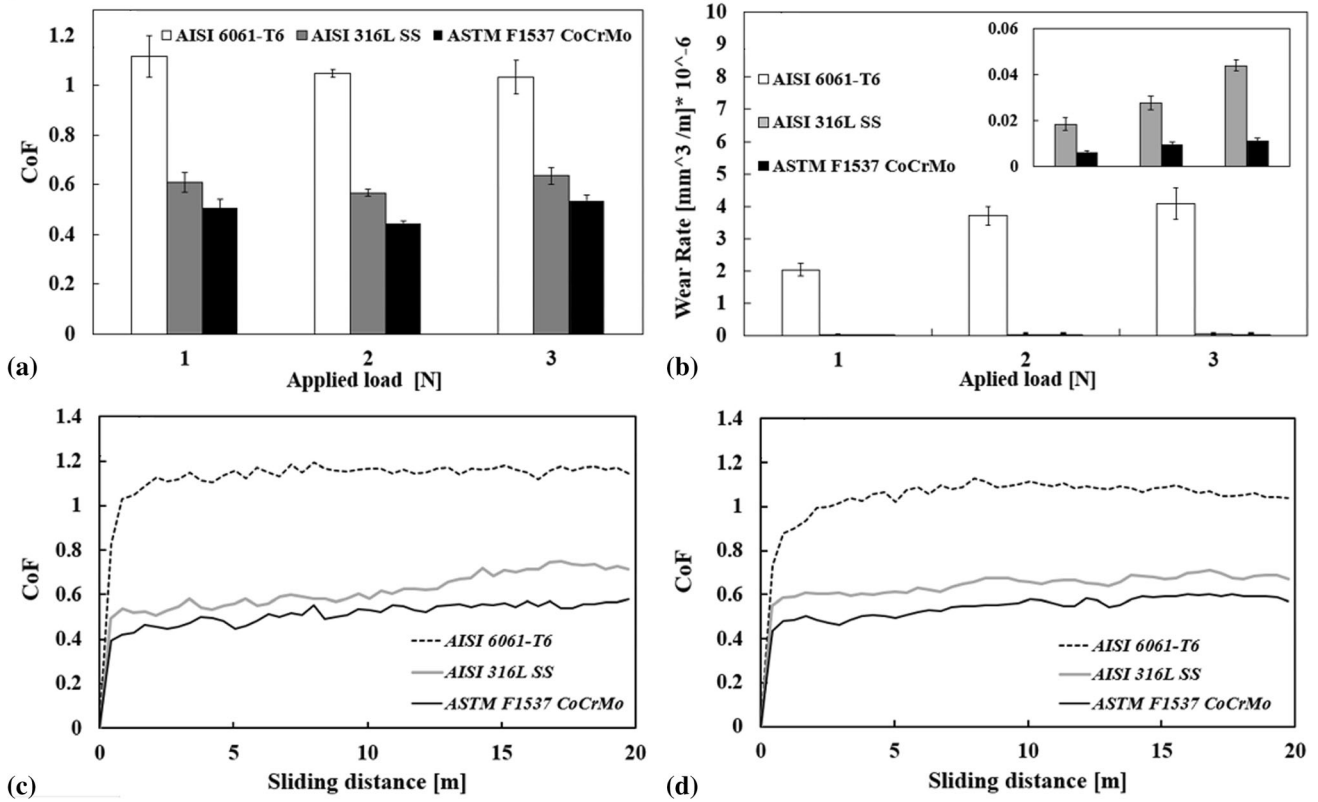
Fig. 6 SEM images from typical wear scars obtained under MLC condition for the materials at 3 N: (a) AISI 316L SS; (b) ASTM F1537 CoCrMo; (c) AISI 6061-T6

wear patterns found under MHC. However, few grooving marks were also identified in some scars. In addition, ridging was produced in the AISI 316L SS scars at 2 and 3 N and AISI 6061-T6 at the three loads. It has been widely reported that ridging occurs at high loads and/or MLC testing for soft materials (Ref 21). Basically, a ridge is formed in the central part of the sliding contact area (highest contact pressure region) due to abrasive particles are restricted to entry into the sliding contact generating two-body abrasion wear instead of rolling abrasion. The wear rates obtained at MLC were considerably lower than those obtained under MHC for all materials. Ridging effect promoted a wear rate decrease with increase of load applied under MLC for AISI 6061-T6 while it promoted a minimal wear rate increase with load applied for AISI 316L SS. In contrast, ASTM F1537 CoCrMo exhibited a consistent wear rate increase with load because ridging was not produced at any load. All materials presented higher CoF values for MLC than those under MHC condition even with the ridge formation. CoF reached mean values of 0.58, 0.50 and 1.35 for ASTM F1537 CoCrMo alloy, AISI 316 SS and AISI 6061-T6, respectively. Thus, it can be assumed that rolling/grooving abrasion generated higher shear forces than rolling abrasion, which promoted CoF increase. In the case of AISI 6061-T6, CoF did not increase with load at MLC opposite to MHC. Besides, it approached the CoF values obtained for MHC at 3 N since the wear patterns for the three loads were almost similar. However, rolling abrasion produced higher wear rates than rolling/grooving according to these findings. Higher wear rates were obtained for the ASTM F1537 CoCrMo alloy with values ranging from 3.5×10^{-7} mm^3/m at 1 N to 10.8×10^{-7} mm^3/m at 3 N compared to the wear rate values of AISI 316L SS which are around 2.5×10^{-7} mm^3/m for the three loads. The wear rate for AISI 6061-T6 aluminum alloy reached values of 17.2×10^{-7} mm^3/m for 1 N but it decreased to 10×10^{-7} mm^3/m at 3 N. Both the negligible increase of wear rate exhibited in AISI

316L SS and the wear rate decrease in AISI 6061-T6 aluminum alloy with load increase is ascribed to ridging formation.

3.3 Coefficient of Friction and Wear Under Wet Sliding

The average CoF and wear rate values at 1, 2 and 3 N, and the CoF behaviors for 1 and 3 N obtained for the materials tested under wet condition are shown in Fig. 7a-d. The SEM images of the typical wear scars produced at 3 N are depicted in Fig. 8a-c. Grooving was found to be the predominant wear mode for AISI 316L SS and ASTM F1537 CoCrMo. It was less severe as that found in MLC tests since the scratches formed under wet condition are much thinner. Those scratches could be generated primarily by the steel ball asperities (two-body abrasion) and secondly by debris detached from the material sample or steel ball producing three-body abrasion in some extent. In the case of AISI 6061-T6, scuffing was found to be the predominant wear mode under this condition. Scuffing occurs when macroscopic adhesions formed at the interface produce plastic shearing of aluminum forming aluminum patches on the counterface and free aluminum debris (Ref 45). In the scuffing process, gross plastic deformation produces local delamination and deep grooves on the scuffed surface (as shown Fig. 8c) which can be formed either by aluminum debris (three-body abrasion) or steel ball' asperities (two-body abrasion). It was observed that water facilitates the aluminum debris entrance into the sliding contact in contrast to those experiments under dry condition as explained later. Although the water was not recycled, the water dropped to the sliding contact tended to be adhered to the ball surface in some extent, so the continuous motion of the ball promotes inherent water auto-recirculation through the test. This process allows the returning of some debris immersed in water to the sliding contact. According to these observations, it is proposed to implement a meticulous continuous cleaning process for the ball that could be suitable for reducing this mechanism if it is desired for other

Fig. 7 (a) Average CoF for the different loads under wet condition; (b) Wear rates for the different loads under wet condition; CoF behavior for wet condition (c) 1 N; (d) 3 N
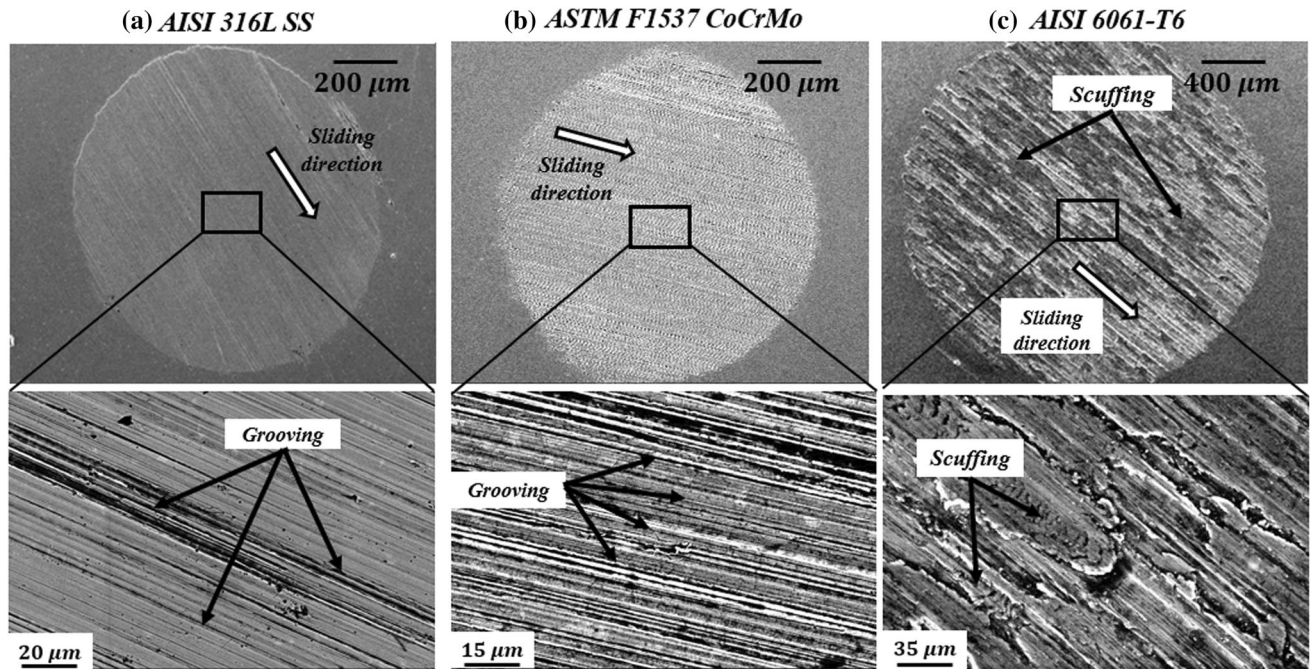
Fig. 8 SEM images from typical wear scars obtained under wet condition for the materials at 3 N: (a) AISI 316L SS; (b) ASTM F1537 CoCrMo; (c) AISI 6061-T6

research purposes. Most of aluminum debris that entrained into the contact could be dragged, deformed plastically and adhered producing very high shear and adhesive forces during sliding. It can be confirmed with the high CoF values obtained for this

material and condition. CoF values were slightly affected by load increase for all materials under wet condition. However, AISI 6061-T6 presented the highest CoF value compared to average CoF values of 0.60 and 0.50 for the AISI 316L SS and

ASTM F1537 CoCrMo alloy, respectively. Wear rates of ASTM F1537 CoCrMo and AISI 316L SS were considerably lower than those obtained at MHC and MLC conditions with values ranging from 0.06×10^{-7} mm^3/m at 1 N to 0.11×10^{-7} mm^3/m at 3 N for the CoCrMo alloy and from 0.18×10^{-7} mm^3/m at 1 N to 0.43×10^{-7} mm^3/m at 3 N for the AISI 316L SS. The wear rates of AISI 6061-T6 were higher than those obtained under MLC condition reaching values from 20.2×10^{-7} mm^3/m at 1 N to 40.9×10^{-7} mm^3/m at 3 N. Scuffing on AISI 6061-T6 promoted a significant higher wear rate than those obtained for ASTM F1537 CoCrMo and AISI 316L SS by grooving under wet condition.

### 3.4 Coefficient of Friction and Wear Under Dry Sliding

The average CoF and wear rate values at 1, 2 and 3 N, and CoF behavior for 1 and 3 N obtained for all tested materials under dry condition are illustrated in Fig. 9a-d. The SEM images from the wear scars obtained at 3 N are shown in Fig. 10a-c. Several grooving marks were found in the scars from all tested materials, but they were slighter than those obtained under MLC and wet condition. Dry sliding produced some debris due to wear. Although it could be believed that debris fall once they are detached from the sample, many of them are adhered or engaged to the ball surface and are returned to the sliding interface by the continuous ball rotation. It can be evidenced by the accumulation of debris identified at the superior region of a wear scar contour of the AISI 6061-T6 by EDS analyses, as shown in Fig. 11. In this case, the debris got embedded due to the material's softness in contrast to ASTM F1537 CoCrMo and AISI 316L SS which have high hardness.

However, debris generated by dry condition do not entry and move as freely at the interface as under MLC or wet condition since the sliding surfaces are not separated by any lubricant film. So, it can be assumed that grooving caused by steel ball surface asperities (two-body abrasion) was the main wear mode for dry condition. The wear rates produced under this condition were the lowest for all materials and loads. The wear rate values ranged from 0.01×10^{-7} mm^3/m at 1 N to 0.03×10^{-7} mm^3/m at 3 N for ASTM F1537 CoCrMo. The wear rate values for the AISI 316L SS were from 0.03 mm^3/m at 1 N to 0.07×10^{-7} mm^3/m at 3 N meanwhile for the AISI 6061-T6 aluminum alloy were from 0.7×10^{-7} mm^3/m at 1 N to 1.3×10^{-7} mm^3/m at 3 N. It is related to the hardness of the ball since it is lower than that of SiC particles interacting in the sliding contact under MHC and MLC, or even, those detached debris from AISI 316L SS and ASTM F1537 CoCrMo under wet condition. CoFs obtained under dry condition were also the lowest for all materials tested with values of 0.30, 0.33 and 0.35 for the ASTM F1537 CoCrMo, AISI 316 SS and AISI 6061-T6, respectively. These values are comparable with those obtained in some studies carried out using the same materials under dry sliding conditions. For example, Campos et al. (Ref 46) evaluated the tribology performance of the ASTM F1537 CoCrMo alloy against Al$_2$O$_3$ balls in dry sliding using a reciprocating friction tester with applied loads of 5, 10, 15 and 20 N obtaining an CoF value around 0.4. Cuau et al. (Ref 47) obtained a CoF of 0.35 for the ASTM F15-12 CoCrMo alloy against Al$_2$O$_3$ balls in dry sliding at applied load of 40 N. Li et al. (Ref 48) evaluated the performance of an AISI 316L SS manufactured by selective laser melting against AISI 52100 steel balls under dry sliding at applied loads of 10, 20 and 30 N
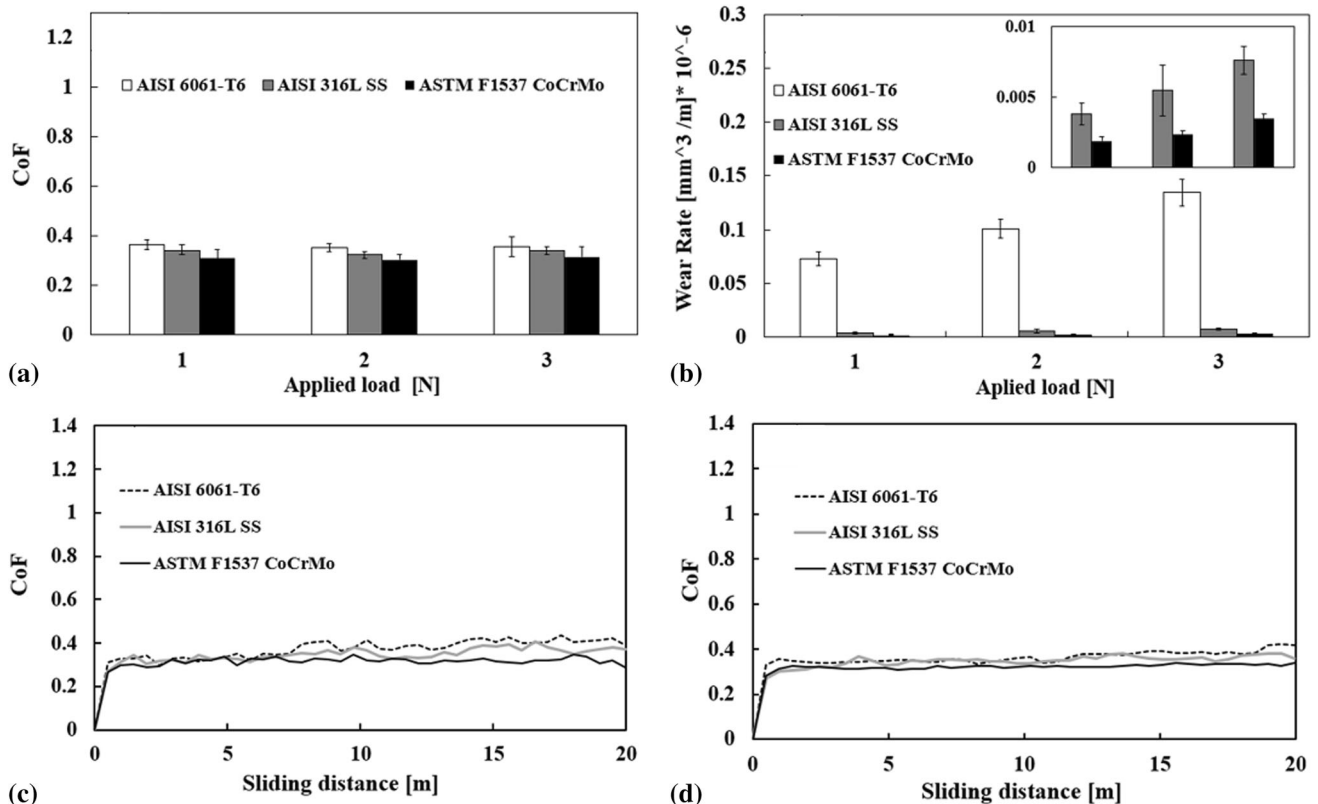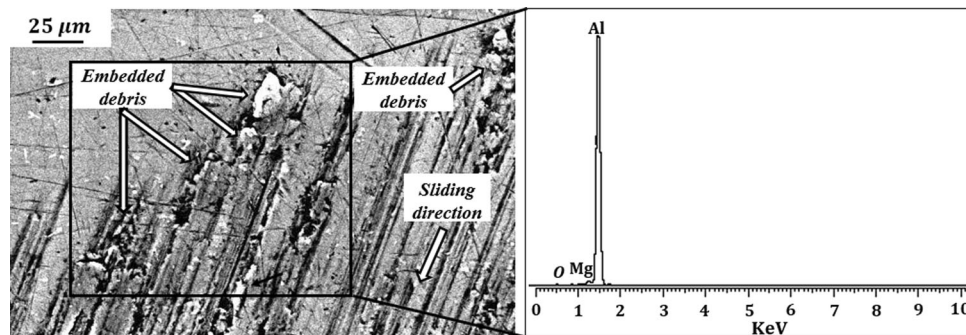

Fig. 9 (a) Average CoF for the different loads under dry condition; (b) Wear rates for the different loads under dry condition; CoF behavior for dry condition (c) 1 N; (d) 3 N
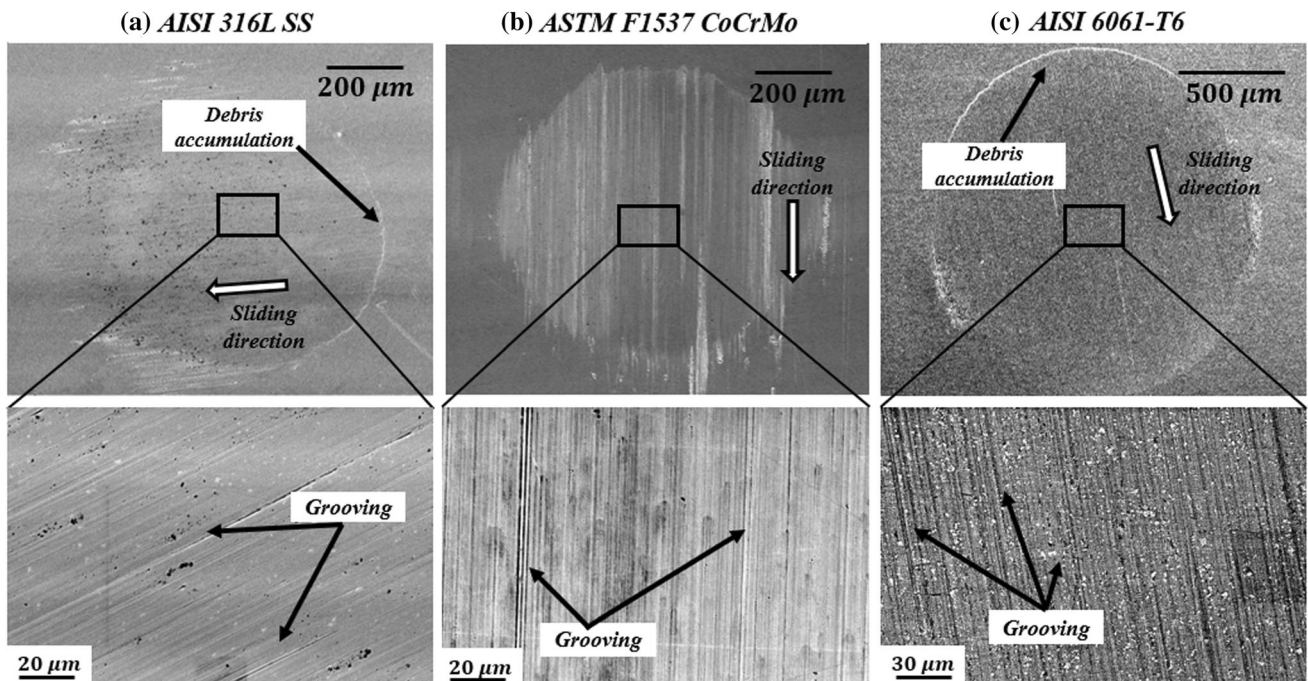
Fig. 10 SEM images from typical wear scars obtained under dry condition for the materials at 3 N: (a) AISI 316L SS; (b) ASTM F1537 CoCrMo; (c) AISI 6061-T6

Fig. 11 EDS analysis in AISI 6061-T6 Aluminum alloy for dry condition

Table 3 Summary of CoF, wear rate and mode results obtained

Material	Load [N]	MHC			MLC			Wet			Dry		
		CoF	WR	WM	CoF	WR	WM	CoF	WR	WM	CoF	WR	WM
CoCrMo	1	0.37	0.46	RA	0.56	0.35	RA/G	0.50	0.006	G	0.30	0.001	G
alloy	2	0.37	0.95	RA	0.57	0.72	RA/G	0.46	0.009	G	0.30	0.002	G
	3	0.41	1.34	RA	0.60	1.08	RA/G	0.53	0.011	G	0.31	0.003	G
Stainless steel	1	0.37	0.71	RA	0.54	0.25	RA/G	0.60	0.018	G	0.33	0.003	G
	2	0.35	1.29	RA	0.48	0.26	RA/G/R	0.58	0.027	G	0.32	0.005	G
	3	0.39	1.60	RA	0.46	0.32	RA/G/R	0.63	0.043	G	0.34	0.007	G
Aluminum alloy	1	0.44	3.70	RA	0.59	1.72	RA/G /R	1.10	2.02	S	0.36	0.07	G
	2	0.41	6.73	RA	0.59	1.37	RA/G/R	1.00	3.71	S	0.35	0.10	G
	3	0.56	8.37	RA	0.58	1.00	RA/G/R	1.00	4.09	S	0.35	0.13	G

WR, Wear Rate ($\times 10^{-6}$ mm^3/m); **WM**, Wear Mode; **RA**, Rolling abrasion; **R**, Ridge; **G**, Grooving; **S,** Scuffing

obtaining CoF values about 0.42. Chen et al. (Ref 49) obtained CoF values about 0.44 for an Aluminum-Silicon alloy against nodular cast iron pins under dry sliding condition at applied load of 20 N. The whole data of CoF, wear rates and modes obtained for all materials are summarized in detail in Table 3. Considering that wear progression in the test samples promotes

wear crater depth increase, it is possible that load applied changes, in some extent, through the test since the L-shaped arm tends to lose the initial position from the no-wear initial condition. Measuring load applied dynamically in the micro-abrasion tester would be valuable for getting deeper tribological analysis which is subject of further research in our research group.

4. Conclusions

- The findings reported and discussed in this work demonstrated that wear mode had a considerable effect on wear rate, but also, on CoF in the metallic materials tested.
- Pure rolling abrasion generated the highest wear rates for all the materials and loads tested.
- Mixed rolling abrasion/grooving produced higher CoFs, but lower wear rates than those produced by pure rolling abrasion.
- Wet sliding abrasion produced grooving patters for the ASTM F1537 CoCrMo alloy and AISI 316L stainless steel while it produced scuffing for the AISI 6061-T6 aluminum alloy. It also promoted the highest CoFs for AISI 316L stainless steel and AISI 6061-T6 aluminum alloy.
- Dry sliding abrasion generated grooving patterns for all materials and loads. It also promoted the lowest CoFs and wear rates for all materials and loads tested.
- The tester used was found to be very useful, practical and appropriated as an efficient tool for CoF evaluation of different tribo-pairs and conditions. Consistent reproduction of specific wear modes and good reproducibility were achieved with relative ease.

References

1. G.B. Stachowiaka, G.W. Stachowiaka, and O. Celliers, Ball-Cratering Abrasion Tests of High-Cr White Cast Irons, *Tribol. Int.*, 2005, **38**, p 1076–1087
2. M.T. Mathew, M.M. Stack, B. Matijevic, L.A. Rocha, and E. Ariza, Micro-Abrasion Resistance of Thermochemically Treated Steels in Aqueous Solutions: Mechanisms, Maps, Materials Selection, *Tribol. Int.*, 2008, **41**, p 141–149
3. F. Marques, W.M. da Silva, J.M. Pardal, S.S.M. Tavares, and C. Scandian, Influence of Heat Treatments on the Micro-Abrasion Wear Resistance of a Superduplex Stainless Steel, *Wear*, 2011, **271**, p 1288–1294
4. P. Vale Antunes and A. Ramalho, Study of Abrasive Resistance of Composites for Dental Restoration by Ball-Cratering, *Wear*, 2003, **255**, p 990–998
5. G.B. Stachowiak and G.W. Stachowiak, Tribological Characteristics of WC-Based Claddings Using a Ball-Cratering Method, *Int. J. Refract. Met. H.*, 2010, **28**, p 95–105
6. S. Sharifi, M.M. Stack, L. Stephen, Wang-Long Li, and Moo-Chin Wang, Micro-Abrasion of Y-TZP in Tea, *Wear*, 2013, **297**, p 713–721
7. M.J. Ibáñez, J. Gilabert, M. Vicent, P. Gómez, and D. Muñoz, Determination of the Wear Resistance of Traditional Ceramic Materials by Means of Micro-Abrasion Technique, *Wear*, 2009, **267**, p 2048–2054
8. M. Sampaio, M. Buciumeanu, B. Henriques, Filipe S. Silva, J.C.M. Souza, and J.R. Gomes, Comparison Between PEEK and Ti6Al4V Concerning Micro-Scale Abrasion Wear on Dental Applications, *J. Mech. Behav. Biomed. Mater.*, 2016, **60**, p 212–219
9. L.I. Farfán-Cabrera, E.A. Gallardo-Hernández, C. Sedano de la Rosa, and M. Vite-Torres, Micro-Scale Abrasive Wear of Some Sealing Elastomers, *Wear*, 2017, **376–377**, p 1347–1355
10. J. Batista, M. Joseph, C. Godoy, and A. Matthews, Micro-Abrasion Wear Testing of PVD TiN Coatings on Untreated and Plasma Nitrided AISI, H13 Steel, *Wear*, 2002, **249**, p 971–979
11. F. Silva, R. Martinho, and A. Baptista, Characterization of Laboratory and Industrial CrN/CrCN/Diamond-Like Carbon Coatings, *Thin Solid Films*, 2014, **550**, p 278–284
12. C.D. Resendiz-Calderon et al., Micro-Abrasion Wear Resistance of Borided 316L Stainless Steel and AISI, 1018 Steel, *J. Mater. Eng. Perform.*, 2017, **26**, p 5599–5609
13. K.L. Rutherford and I.M. Hutching, A Micro-Abrasive WEAR Test, with Particular Applications to Coated Systems, *Surf. Coat. Tech.*, 1996, **79**, p 231–239
14. K.L. Rutherford and I.M. Hutchings, Theory and Application of a Micro-Scale Abrasive Wear Test, *J. Test Evalut.*, 1997, **25**(2), p 250–260
15. R.I. Trezona, D.N. Allsopp, and I.M. Hutchings, Transitions Between Two-Body and Three-Body Abrasive Wear: Influence of Test Conditions in the Microscale Abrasive Wear Test, *Wear*, 1999, **225–229**, p 205–214
16. K. Adachi and I.M. Hutchings, Wear-Mode Mapping for the Micro-Scale Abrasion Test, *Wear*, 2003, **255**, p 23–29
17. G.B. Stachowiak and G.W. Stachowiak, Wear Mechanisms In Ball-Cratering Tests with Large Abrasive Particles, *Wear*, 2004, **256**, p 600–607
18. J.T. Burwell, Survey of Possible Wear Mechanisms, *Wear*, 1957, **1**(2), p 119–141
19. W.M. da Silva and J.D.B. de Mello, Using Parallel Scratches to Simulate Abrasive Wear, *Wear*, 2009, **267**, p 1987–1997
20. W.M. da Silva, H.L. Costa, and J.D.B. de Mello, Superimposition of Interactions: A New Approach to Simulating Abrasive Wear Mechanisms, *Wear*, 2011, **271**, p 977–986
21. R. Trezona and I.M. Hutchings, Three-Body Abrasive Wear Testing of Soft Materials, *Wear*, 1999, **209–221**, p 233–235
22. D.N. Allsopp, R.I. Trezona, and I.M. Hutchings, The Effects of Ball Surface Condition in the Micro-Scale Abrasive Wear Test, *Tribol. Lett.*, 1998, **5**, p 259–264
23. M.G. Gee et al., Progress Towards Standardization of Ball Cratering, *Wear*, 2003, **255**, p 1–13
24. Y. Kusano, K. Van Acker, and I.M. Hutchings, Methods of Data Analysis for the Micro-Scale Abrasion Test on Coated Substrates, *Surf. Coat. Technol.*, 2004, **183**, p 312–327
25. C. Leroy, K. Schiffmann, V. Acker, and J. Stebut, Ball Cratering an Efficient Tool for 3 Body Microabrasion of Coated Systems, *Surf. Coat. Technol.*, 2005, **200**, p 153–156
26. Y. Kusano and I.M. Hutchings, Sources of Variability in the Free-Ball Micro-Scale Abrasion Test, *Wear*, 2005, **258**, p 313–317
27. K. Adachi and I.M. Hutchings, Sensitivity of Wear Rates in the Micro-Scale Abrasion Test to Test Conditions and Material Hardness, *Wear*, 2005, **258**, p 318–321
28. M.G. Gee, Results From an Interlaboratory Exercise to Validate the Micro-Scale Abrasion Test, *Wear*, 2005, **259**, p 27–35
29. F.J.G. Silva, R.B. Casais, R.P. Martinho, and A.P.M. Baptista, Role of Abrasive Material on Microabrasion Wear Tests, *Wear*, 2011, **271**, p 2632–2639
30. M.G. Gee and M.J. Wicks, Ball Crater Testing for the Measurement of the Unlubricated Sliding Wear of Wear-Resistant Coatings, *Surf. Coat. Technol.*, 2000, **133–134**, p 376–382
31. R.C. Cozza, D.K. Tanaka, and R.M. Souza, Friction coefficient and abrasive wear modes in ball-cratering tests conducted at constant normal force and constant pressure—Preliminary results, *Wear*, 2009, **267**, p 61–70
32. R.C. Cozza, A Study on Friction Coefficient and Wear Coefficient of Coated Systems Submitted to Micro-Scale Abrasion Tests, *Surf. Coat. Technol.*, 2013, **215**, p 224–233
33. R.C. Cozza, Influence of the Normal Force, Abrasive Slurry Concentration and Abrasive Wear Modes on the Coefficient of Friction in Ball-Cratering Wear Tests, *Tribol. Int.*, 2014, **70**, p 52–62
34. Y. Peng et al., Friction and Wear of Liner and Grinding Ball in Iron Ore Ball Mill, *Tribol. Int.*, 2017, **115**, p 506–517

35. P. Sinnett-Jones, J. Wharton, and R. Wood, Micro-Abrasion-Corrosion of a CoCrMo Alloy in Simulated Artificial Hip Joint Environments, *Wear*, 2005, **259**, p 898–909

36. J. Bello, R. Wood, and J. Wharton, Synergistic Effect of Micro-Abrasion-Corrosion of UNS S30403, S31603 and S32760 Stainless Steels, *Wear*, 2007, **263**, p 149–159

37. D. Sun, R. Wharton, and R. Wood, Micro-Abrasion Mechanism of Cast CoCrMo in Simulated Body Fluids, *Wear*, 2009, **267**, p 1845–1855

38. D. Sun, J. Wharton, and R. Wood, Micro-Abrasion-Corrosion of Cast CoCrMo—Effects of Micron And Sub-Micron Sized Abrasives, *Wear*, 2009, **267**, p 52–60

39. M. Stack, J. Rodling, M. Mathew, H. Jawan, W. Huang, G. Parck, and C. Hodge, Micro-Abrasion-Corrosion of a Co-Cr/UHMWPE Couple in Ringer's Solution: An Approach to Construction of Mechanism and Synergism Maps for Application to Bio-Implants, *Wear*, 2010, **269**, p 376–382

40. W. Huang, G. Wang, and Z. Zheng, Micro-Abrasion-Corrosion of Ti6Al4V Alloy in Simulated Artificial Hip Joint Environment, *Advanced Tribology, Proceedings of CIST2008 & ITS-IFToMM2008*, J. Luo, Y. Meng, T. Shao, and Q. Yzhao, Ed., Springer, China, 2010, p 1005–1010

41. H. Costa, M. Ardila, W. Labiapari, W. Silva, and J.D. Mello, Effect of Surface Topography on the Dynamics of the Abrasive Particles During Micro-Abrasion, *Wear*, 2015, **324–325**, p 129–139

42. W. Oliver and G. Pharr, An Improved Technique for Determining Hardness and Elastic Modulus Using Load and Displacement Sensing Indentation Experiments, *Mater. Res.*, 1992, **7**(6), p 1564–1583

43. I. Hutchings and P. Shipway, *Tribology Friction and Wear of Engineering Materials*, 2nd ed., Elsevier, Amsterdam, 2017, p 114–119

44. J.A. Williams and A.M. Hynsica, Mechanims of Abrasive Wear in Lubricated Contacts, *Wear*, 1992, **152**, p 57–74

45. Hyung Yoon, Todor Sheiretov, and Cris Cusano, Scuffing Behavior of 390 Aluminum Against Steel Under Starved Lubrication Conditions, *Wear*, 2000, **237**, p 163–175

46. I. Campos-Silva et al., Dry Sliding Wear Resistance of Cobalt Boride Coatings Formed on ASTM F1537 Alloy, *J. Mater. Eng. Perform.*, 2019, **28**(4), p 2399–2410

47. C.A. Cuao-Moreu, E. Hernández-Sanchéz, M. Alvarez-Vera, E.O. Garcia-Sanchez, A. Perez-Unzueta, and M.A.L. Hernandez-Rodriguez, Tribological Behavior of Borided Surface on CoCrMo Cast Alloy, *Wear*, 2019, **426**, p 204–211

48. H. Li, M. Ramezani, M. Li, C. Ma, and J. Wang, Tribological Performance of Selective Laser Melted 316L Stainless Steel, *Tribol. Int.*, 2018, **128**, p 121–129

49. L. Chen, Z. Liu, B. Wang, Q. Song, Y. Wan, and L. Chen, Surface Characterization and Tribological Performance of Anodizing Micro-Textured Aluminum-Silicon Alloys, *Materials (Basel)*, 2019, **12**(11), p 1862